Zonal detached-eddy simulation of tip-leakage flow sensitivity for a compressor rotor

Christophe Montsarrat, Jérôme Boudet, Julien Marty, Eric Lippinois

ZONAL DETACHED-EDDY SIMULATION OF TIP-LEAKAGE FLOW SENSITIVITY FOR A COMPRESSOR ROTOR

Christophe Montsarrat[1], *Jérôme Boudet*[2], *Julien Marty*[3], *Eric Lippinois*[4]

[1] Fluid Mechanics and Acoustics Laboratory (LMFA), Turbomachinery Department, Ecole Centrale de Lyon, Ecully, France, christophe.montsarrat@ec-lyon.fr
[2] Fluid Mechanics and Acoustics Laboratory (LMFA), Turbomachinery Department, Ecole Centrale de Lyon, Ecully, France, jerome.boudet@ec-lyon.fr
[3] ONERA, the French Aerospace Lab, Meudon, France, julien.marty@onera.fr
[4] Safran Aircraft Engines, Moissy-Cramayel, France, eric.lippinois@safrangroup.com

ABSTRACT

The dependence of the tip-leakage flow to the tip gap size is investigated on the third rotor of a high-pressure axial compressor. Three tip clearances are simulated with a hybrid RANS/LES approach at the nominal operating point with the objective of resolving better the vortical structures in the tip region. The numerical results are in fair agreement with the experiment in the tip region, for the largest gap. The structures depicted in the simulations indicate stronger vortical structures with the larger gaps and a significant blockage induced by them. The results indicate that a double leakage takes place about midchord for the larger gap, changing completely the dynamics of the leakage flow, likely to be causing a vortex breakdown. This also occurs for the intermediate gap but with a lower intensity and no breakdown. The power spectral density at the trailing edge at the tip finally illustrates the higher energy levels for increasing gap values.

KEYWORDS

Tip-leakage flow, ZDES, Vorticity, Compressor

NOMENCLATURE

TLV	Tip-leakage vortex	k	Turbulent kinetic energy (TKE)
TLF	Tip-leakage flow	Q	Mass flow rate
TSV	Tip-separation vortex	r_{tip}	Radius of the third rotor blade tip
RANS	Reynolds-averaged Navier-Stokes	$U_{tip} = r_{tip}\omega$	Speed at the tip
LES	Large-Eddy Simulation	c_a	Axial chord
ZDES	Zonal-Detached Eddy Simulation	PSD	Power spectral density
μ_t/μ	Eddy-to-molecular viscosity ratio	t	Thickness of the blade
f_d	Protection function	τ	Tip gap size
$\omega = 11543rpm$	Revolution speed of the rotor	$St_L = \frac{fL}{U_{tip}}$	Strouhal number based on the length scale L

1 INTRODUCTION

Tip-leakage flow (TLF) can be found at the tip of compressor and turbines. This well-known phenomenon in turbomachinery is responsible for large losses and subsequent performance reduction. For a compressor, not only does it contribute to nearly thirty percent of the losses [6] but it is also involved in the onset of instabilities [22] [3], reducing the operating range.

1.1 Topology of TLF

Rains' model [17] is one of the first models developed for TLF. Assuming the pitchwise gradients are much greater than streamwise, the flow can be divided into two main regions: one

within the clearance where a *vena contracta* forms due to the acceleration of the fluid, another where the leakage flow rolls up and eventually detaches from the blade suction side to form the tip-leakage vortex (TLV). This TLV is a significant contribution to the losses in the passage. The TLV is supplied all along the chord by tip-separation vortices (TSV), formed within the gap [13]. Along with the TLV, induced vortices also form, with an opposite sense of rotation. They are generated by the interaction of the TLV with the casing boundary layer. Those vortices develop and diffuse through the passage. Disturbed by the presence of these three-dimensional structures, the deflection produced by the rotor is disturbed and part of the energy is lost in the conversion of the axial component of the velocity into a pitchwise component. The size, the intensity and the trajectory of the TLV strongly affect the flow conditions in the tip region and must be captured carefully to achieve a better understanding of TLF. The most influent parameters of the TLV characteristics, identified in the literature, are the tip gap size [8] [7], the loading of the blade [18] [14], and the casing boundary layer characteristics [1] [12]. This paper is intended to focus on the former with the use of hybrid RANS/LES simulations on a compressor rotor.

1.2 Simulating TLF

Several sensitivity studies have been done regarding TLF with RANS approaches. For example, the investigation of Hewkin-Smith *et al.* [11] provides a good explanation on the flow topology in the tip region that leads to rotating stall, a well-known instability encountered in compressors [4]. Their study shows that there exists an optimal tip gap size corresponding to a minimal flow coefficient achievable by the machine and therefore to a larger operating range. Their explanation lies in two different flow topologies depending on the gap size, compensating each other for the optimal tip gap size: the one described with Rains' model for larger gaps, and another one where a corner separation takes place when the tip gap is very small. Other RANS studies have allowed capturing better the mean behaviour of the TLV for different loading conditions, including the relative motion of the casing [23] [12] but also the unsteadiness associated to the TLV, especially due to vortex wandering [25].

Nevertheless, the capabilities of RANS are limited when it comes to separated and secondary flows, and a finer resolution is required to go further in the understanding of the phenomenon. In particular, very few sensitivity studies were carried out on TLF with large-eddy simulations (LES). You *et al.* [24] identified clearly the structures in the tip region on a turbomachinery cascade with the help of LES, for a fixed tip gap size. They showed that the TLV was the most energetic vortical structure in the tip region and linked more clearly the strong levels of vorticity to the turbulent fluctuations due to both the tip-leakage jet through the clearance and the TLV [24]. The effects induced by a large rotor tip gap (4% of the rotor span) were investigated by Hah [10] on a 1.5 stage axial compressor, based on LES and PIV results for different operating points, compared to the results obtained for a small clearance (0.8% of the rotor span). This revealed the occurrence of a *double-leakage tip clearance flow* at all operating points for the larger gap. This is defined by the impingement of the TLV of the adjacent blade on the pressure side of the current blade, inducing an interaction between this TLV and the clearance flow. This interaction led to the breakdown of the vortex. No double-leakage tip clearance flow nor any vortex breakdown were observed with the small gap.

The simulations of Riéra *et al.* [18] on the first rotor of a high-pressure axial-flow compressor validated the Zonal Detached-Eddy Simulation (ZDES) approach on these configurations, and demonstrated the benefits of ZDES over RANS for two different loading conditions. The

present study is a follow-up to the study of Riéra. The paper investigates the tip gap size effect on the third rotor of the same high-pressure compressor with a ZDES resolution. A previous study was published on the same configuration to assess the benefits of ZDES with respect to RANS [16]. A sensitivity analysis is here carried out for three different tip gap sizes. First, the numerical settings of the simulations are presented, along with the experimental setup used. Second, the numerical results are compared to the experimental measurements. Finally, a tip flow analysis is conducted to compare the flow topology and the characteristics of TLF depending on the tip gap size.

2 PRESENTATION OF THE STUDY

2.1 Experimental setup

The experimental rig chosen for reference in this study is a 3.5-stage high-pressure compressor, CREATE, whose meridian view is shown in Figure 1. The present study focuses on the third rotor, chosen for the intensity of the phenomena observed experimentally, especially regarding TLF. The TLV of this rotor is more energetic in the different operating conditions tested (peak efficiency and near stall) than for the other rotors [2]. The large gap/span ratio ($> 2.5\%$) on this rotor contributes to that effect. Steady probe measurements in the planes colored in the figure, along with Laser Doppler Anemometry (LDA) measurements, will be used for the comparison between the simulations and the experiment. The study is restricted to the experimental nominal operating point as the aim of the paper is to analyze the characteristics of the TLV at peak efficiency conditions, influenced by the tip gap size. Table 1 summarizes the three tip gap values chosen, normalized by the largest, which corresponds to that of the experimental rig. The smallest value has been chosen very small to investigate a possible casing corner separation, as described in the introduction.

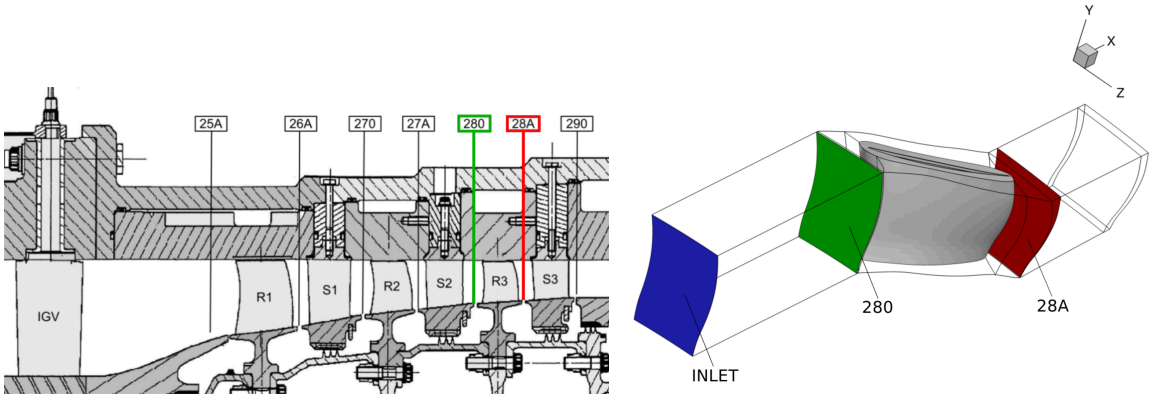

(a) Meridian view (b) Computational domain

Figure 1: **Meridian view of CREATE and computational domain used for the simulations. The planes upstream and downstream of the third rotor are indicated in green** (280) **and red** $(28A)$**. The blue one corresponds to the inlet plane of the simulations.**

2.2 Numerical study

One passage of the third rotor is simulated. Such a choice comes from the numerical resolution used for the study. Indeed, although ZDES is less demanding than LES in terms of grid resolution [5], the computational domain nevertheless requires more than 100×10^6 elements on one passage of the row. Table 2 gives the mesh requirements required by ZDES compared

	CREATE A	CREATE B	CREATE C
Tip gap ratio	1	0.77	0.27
Number of elements in the clearance	49	49	33
First grid element size	1 μm	1 μm	1 μm
Expansion ratio	1.15	1.13	1.17

Table 1: **Tip gap values normalized by the largest gap value for the parametric study done here.**

	Δx^+	y^+	Δz^+
RANS	500	1	1000
ZDES	200	1	100
LES	50	1	15

Table 2: **Mesh requirements in wall units [5].**

to RANS and LES, in wall units. The size of the computational grid would be about one order of magnitude larger for a wall-resolved LES. The inlet boundary condition is located $1.5c_a$ upstream of plane 280 and the outlet is placed $1.5c_a$ downstream of plane $28A$ to reduce numerical interference from the boundary conditions. The grid is also stretched downstream of plane $28A$ to limit wave reflections.

The numerical simulations have been performed with *elsA*, a software developed by ONERA and co-owned by Safran and Airbus. The Navier-Stokes equations are solved on multi-block structured grids with a cell-centered finite volume approach. In order to reduce the artificial dissipation in the ZDES simulations, the AUSM+P scheme [19] is used for the inviscid fluxes. The viscous fluxes are discretized with a second-order centered formulation. The time discretization relies on the second-order Gear scheme with 15 subiterations, to ensure a decrease of more than one order of magnitude on the residuals for each physical time step, which is set to $\Delta t = 0.7\,\mu s$. The unsteady fields are time-averaged over 20 blade passaging periods, also representing about 20 advection periods $T_{adv} = c_a/U_{tip}$ (calculated on the axial chord c_a), for a sufficient convergence of the first and second order statistics of the conservative variables. The computations each run over 375 cores. Overall, the CPU cost is about 600000 hours.

The ZDES approach is an extension of the DES deriving from Spalart-Allmaras turbulence model [21]. This hybrid method consists in simulating the attached boundary layers with an unsteady RANS approach and the rest of the flow with LES. This is particularly advantageous when boundary-layer separations occur, since the method has been designed to switch to LES from the separation point, in order to deal with the limitations of RANS regarding separated flows. Although extended to other turbulence models [15], the ZDES formulation used for the present study is the original one and most mature, validated by Riéra on the first rotor of CREATE, associated to the Spalart-Allmaras model (SA model). The second mode of ZDES is used to ensure the RANS treatment of the attached boundary layers, where it is generally well-adapted. The principle of the method and the details of its application are thoroughly described in Deck's paper [5].

The boundary condition at the inlet is based on the injection of the following five values in the absolute frame of reference: total pressure, total temperature, pitchwise flow angle α, meridian flow angle φ, and turbulent value $\tilde{\nu}$ from the SA model. A radial equilibrium is applied on the outlet condition with a pivot static pressure that can be varied. An adiabatic no-slip condition is applied to the walls (blade skin and endwalls). A periodicity condition is finally imposed on the sides of the domain. The inlet and outlet flow quantities are extracted from a 3-stage RANS simulation in planes 280 and $28A$, calibrated on the experimental nominal point. The boundary conditions are the same for the three simulations with different tip gaps.

Because the computational domain is reduced around the third rotor, the inflow conditions injected are deformed between the inlet plane and plane 280 (resp. the outflow conditions between the outlet plane and plane $28A$). They were consequently recalibrated in a RANS simulation over the same computational domain.

3 RESULTS AND DISCUSSIONS

3.1 Comparisons with the experiment

Before developing the sensitivity study on the tip gap size, the results from the ZDES simulations have to be compared to the measurements. In the experiment, the tip gap size corresponds to the configuration CREATE A, which must be used as a reference for the comparisons. The performance of the rotor is presented in Table 3, comparing the three tip gap sizes. The mass flow rate is overestimated by 10% compared to the experiment. The resulting compression ratio is nevertheless acceptable with a 2% difference compared to the experiment. As for the efficiency, the simulation predicts a more efficient compression than the experiment.

These differences can be explained by the fact that the rotor-stator interactions are not accounted for in the isolated rotor simulation: using unsteady inflow conditions could be a source of improvement. Also, the cavities upstream and downstream the rotor are not considered. Another reason is that the total pressure and temperature from the experiment are averaged between 5% and 95% height. Since the average is weighed by the mass flow rate, this could increase the underestimate obtained numerically on the total pressure. The focus in the present study is not in the calibration of the boundary conditions, which could be improved, especially at the outlet, where the resulting static pressure is underestimated. The objective is to compare the influence of the tip gap size on the flow with ZDES. A fair agreement of the flow conditions in the tip region with the experimental measurements, used as a reference, is aimed for.

	CREATE A	**CREATE B**	**CREATE C**
Mass flow rate	1.10	1.11	1.13
Compression ratio	0.978	0.979	0.977
Isentropic efficiency	1.067	1.074	1.083

Table 3: **Performance recap for the three different gaps of the study, normalized by the values of the nominal operating point from the experiment on CREATE A.**

Commenting on the tip gap size influence, closing the gap coherently induces a larger mass flow rate since the TLV, as it will be shown, is less energetic and therefore deviates less the axial component of the velocity. The overall compression ratio is virtually constant but the isentropic efficiency clearly increases with the decrease of the tip gap and show a better efficiency than the experiment for the three cases.

Figure 2a shows the radial profiles of the compression ratio, normalized by the experimental value at nominal point. Compared to the experiment, case A shows an underestimate of the compression ratio of about 2% all over the span, consistently with the global compression ratio calculated. We are here interested in the tip region ($> 80\%$ height) for the analysis, where the comparisons between the experiment and the ZDES are in fair agreement.

Let us now compare the three tip gaps. Overall, the global compression ratio is nearly the same for the three tip gaps but distributes differently spanwise: the largest gap is associated to the largest total pressure deficit in the tip region while the smaller gap yields more compression in the last 10% height near casing. The influence of the gap size is demonstrated down to 70%

height while the rest shows no difference between the three cases. The intermediate gap results in a better compression ratio by about 4% between 70 and 85% height.

It is recalled that the absolute flow boundary conditions are kept constant between the three cases. With the tip gap decrease, the three-dimensional effects in the tip region are less significant, which explains the larger mass flow rate and the increase of the axial velocity in Figure 2b (upstream plane). In the downstream plane $28A$, the axial velocity from CREATE A compares very well to the experimental results in the last 40% height, in terms of gradients and magnitudes. When the tip gap is reduced, the thickness of the low momentum region at tip decreases and the blockage is consequently the lowest with case C, also explaining why the compression ratio is larger in that case.

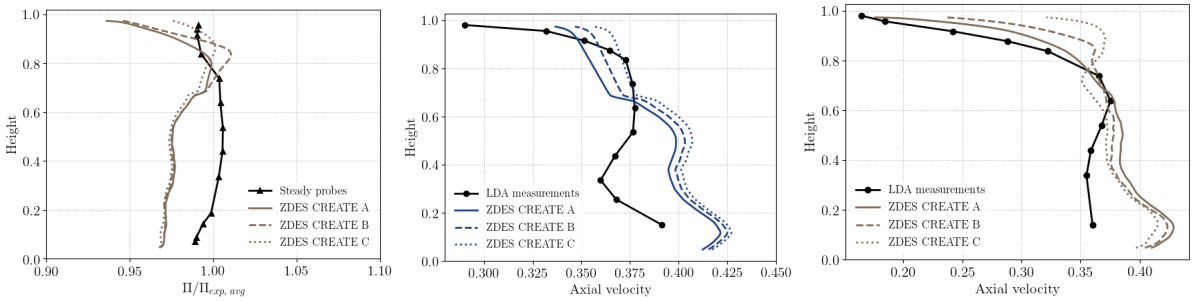

(a) Compression ratio (b) Axial velocity 280 (c) Axial velocity $28A$

Figure 2: **Mean radial profiles from the ZDES simulations and the experiment. The total-to-total compression ratio is measured with pneumatic probes, while the axial velocity is measured with LDA.**

3.2 Tip flow analysis

3.2.1 Flow topology

The topology of the flow is checked in this section through a mean flow analysis. Figure 3 shows an isosurface of a Q-criterion in the tip region, with the same value for the three gaps. The isosurface is colored by normalized helicity, indicating the sense of rotation of the vortices. The topology found in the tip region is classical: the TLV detaches at about 20% c_a from the blade suction side and is fed by the tip-separation vortices (TSV) downstream. The induced vortex (IV) resulting from the interaction of the TLV with the casing boundary layer is also observable in the three cases. The effect of the tip gap size can first be seen through the position of the induced vortex in case C, following a different trajectory with the smallest gap. This suggests that the less intense TLV interacts differently with the boundary layer. In case A, the TLV seems to divide into smaller and smaller structures, which could characterize a TLV breakdown. This breakdown is not observed in the two other cases: in case B, the TLV is still very intense but maintains its structure along the passage. Likewise with case C with much lower intensity.

The question of the LES resolution of the TLV is crucial here. Figure 4 shows two important values to understand how the tip region is treated:

1. The ratio μ_t/μ is classically used in RANS approaches to quantify the turbulent levels of the flow. Indeed, the Boussinesq hypothesis relates the turbulent fluctuations of the flow to the mean velocity gradients through the turbulent eddy viscosity μ_t. A large value of μ_t models large turbulent fluctuations.

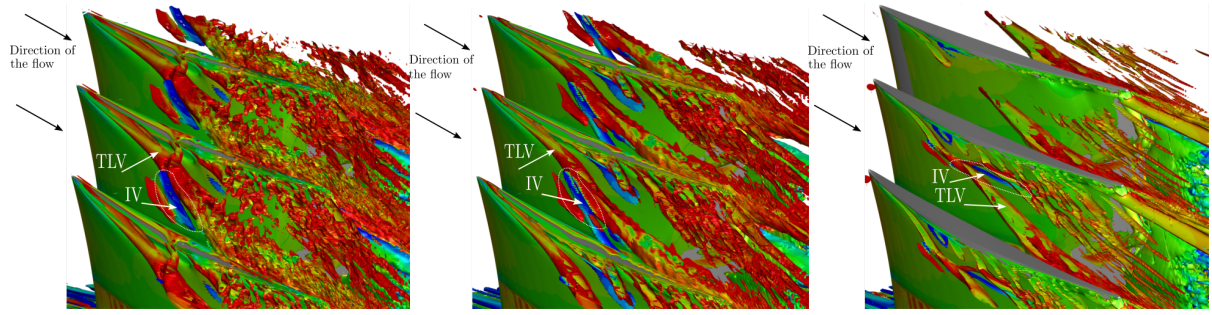

(a) Case A (b) Case B (c) Case C

Figure 3: **Time-averaged isosurface of Q-criterion, colored by normalized helicity from** -1 **(blue) to** 1 **(red).**

2. The sensor f_d introduced in Spalart's DES [20] and in the ZDES formulation used here [5]: $f_d = 0$ indicates a RANS treatment while $f_d = 1$ corresponds to a LES resolution. In-between, there is a grey zone where the eddy viscosity is destroyed and compensated by resolved turbulent fluctuations.

Two main points are observable in the figure. Upstream the row, the casing boundary layer remaining attached, the second mode of the ZDES ensures a RANS treatment of it. Note that the tip gap is completely immersed in the casing boundary layer. The thick boundary layer is then sheared by the rotor and the eddy viscosity levels drop from about $20\%\ c_a$, where the TLV detaches from the suction side of the blade. What the figure shows is that the TLV is completely resolved from its detachment point, with levels of $\mu_t/\mu < 1$ characteristic of subgrid scale levels for LES. Besides, the protection function f_d is greater than 0.99 for the three tip gaps in these zones, confirming the LES resolution of the TLV. Furthermore, it is worth noticing that the extension of the LES region is much larger in case A than in case C, suggesting a more energetic TLV with a larger extension for the largest gap.

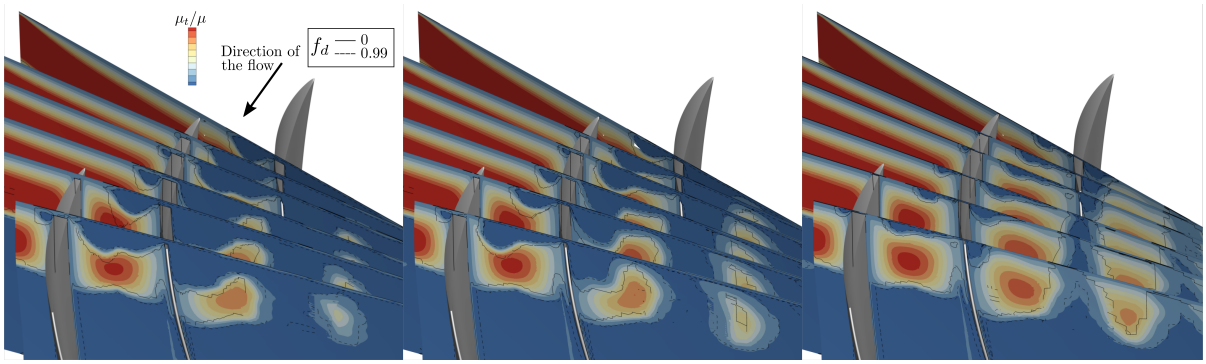

(a) Case A (b) Case B (c) Case C

Figure 4: **Eddy-to-laminar viscosity ratio contours and isolines of the sensor** f_d**. A LES resolution corresponds to** $f_d = 1$ **and a RANS resolution to** $f_d = 0$**. The planes are perpendicular to the suction side at the positions** 0**,** 10**,** 21**,** 40**,** 61 **and** 95 **% of axial chord.**

3.2.2 *Vorticity and TKE*

The vorticity is a major feature of the TLV. The vortex is described as more intense if it is responsible for higher levels of vorticity. Figure 5 shows the evolution of the vorticity magnitude through the passage, illustrating the formation of the TLV and its development once detached from the blade. As already observed with the f_d distribution, the TLV extent is larger for the larger gaps. This is particularly visible between case A and case C. For case C, downstream of the trailing edge in the right-hand side passage, the TLV is rapidly dissipated and generally seems less energetic than in the two other cases. The small structures observed in case A with the Q-criterion are also visible with vorticity, in the plane around 40% c_a where the TLV impacts the pressure side of the neighboring blade. This TLV/blade interaction could explain the higher levels of blockage shown in the radial profile in plane $28A$ for case A, and the breakdown observed with the Q-criterion.

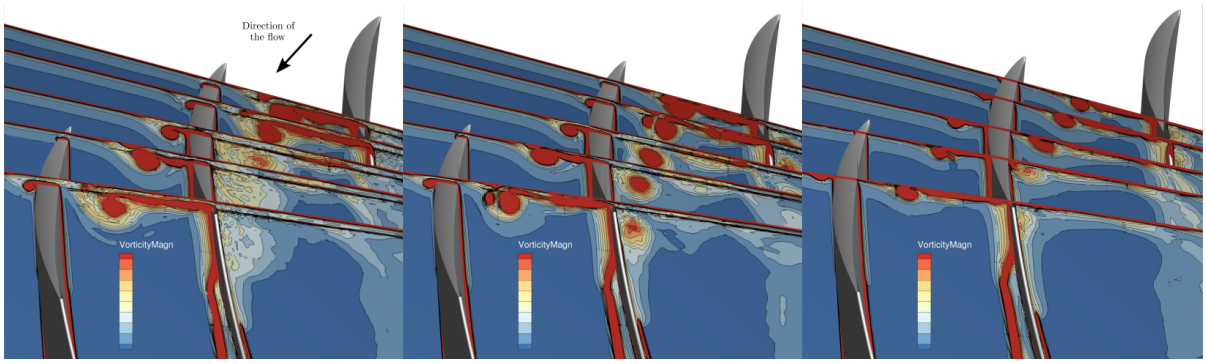

(a) Case A (b) Case B (c) Case C

Figure 5: **Vorticity magnitude evolution through cutting planes perpendicular to the suction side of the blade, for the three tip gaps. The same scale is used in the three cases. The planes are perpendicular to the suction side at the positions** 10**,** 21**,** 40**,** 61 **and** 95 **% of axial chord.**

The energy levels associated to the TLV are directly shown in Figure 6 where the resolved turbulent kinetic energy (TKE) k contours are plotted in terms of turbulent intensity:

$$Tu = \frac{\sqrt{2/3\ k}}{U_{tip}}. \tag{1}$$

As the TLV is completely resolved with LES, only the resolved fluctuations are here displayed, following the track of the TLV, which is then clearly identified. The large intensity of the TLV for the largest gap is observed and can be related to significant losses. In the last plane at the trailing edge, the turbulence levels reach 30% near the core of the TLV, with fluctuations expanding pitchwise in the whole passage with levels greater than 10%. In comparison, in the same plane, cases B and C present lower levels of TKE, the TLV size and intensity being very limited in case C compared to case A. In case B, the TLV is still energetic but situates in-between the two other cases. The TLV/blade interaction taking place from about 40% c_a with the larger gap (case A) seems to have a major influence on the passage blockage. Very high levels of turbulence are observed within the clearance at this axial position compared to the two

other cases, driving the TLV evolution quite differently downstream. The breakdown responsible for the generation of the small vortical structures in case A could probably originate from this interaction. It can be noticed that a TLV/blade interaction also occurs for case B from 60% c_a, with lower intensity than for case A. This interaction is very similar to the double-leakage tip clearance flow described in the introduction. It can be noted that it occurs for nominal flow conditions on the two larger gaps and that it does not on the smaller gap (tip/rotor span $< 1\%$), similarly to Hah's study [10]. Nevertheless, the intermediate gap seems to show that a double-leakage tip clearance flow occurs but does not yield a vortex breakdown, based on the Q-criterion view.

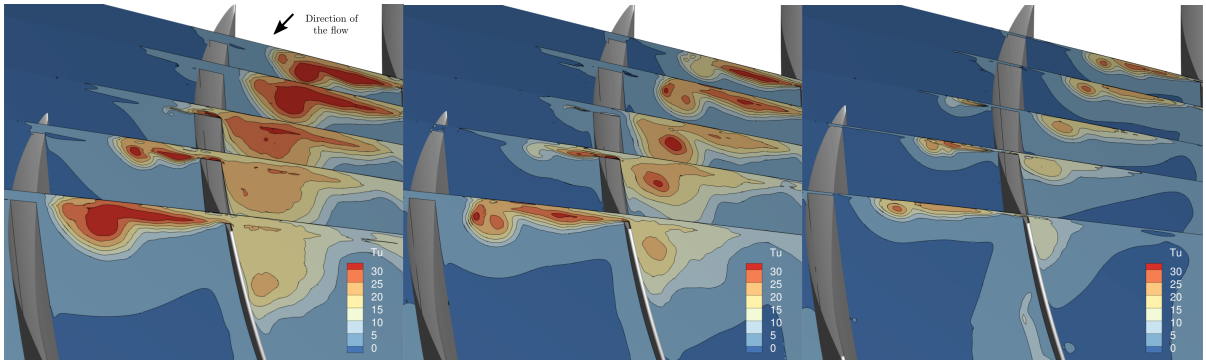

(a) Case A (b) Case B (c) Case C

Figure 6: **Streamwise evolution of the resolved turbulence intensity (in $\%$), in planes perpendicular to the suction side of the blade.**

This phenomenon can also be observed differently on the pitchwise component of the velocity within the clearance. The mean relative tangential velocity W_θ (leakage velocity) is extracted in the clearance above the suction side. Figure 7a indicates the tip clearance zone in red: the leakage velocity is extracted in the continuity of the suction side in the red zone and averaged radially. This processing allows estimating the streamwise evolution of the leakage flow velocity. As shown in Figure 7b, the leakage velocity is almost identical in the first 40% chord between cases A and B, but a major difference can be observed downstream where the magnitude of the leakage velocity suddenly drops in case A. It thus passes from 1.0 to 0.75 in less than 5% chord. It even becomes lower than for case C from this position to the trailing edge. This position roughly corresponds to the beginning of the TLV/blade interaction observed with the resolved TKE for case A. This can explain the sudden leakage velocity drop in magnitude since intense turbulent fluctuations are sucked up in the clearance and are expected to reduce the leakage flow by a local increase of the losses.

In case B, the same abrupt drop appears around midchord but with a lower amplitude (0.1 on the leakage velocity). Similarly, the axial position for case B corresponds approximately to the TLV/blade interaction, around 60% c_a. Nonetheless, the levels of the TKE in the impacting TLV are much lower than for case A, and the leakage flow is slightly reduced at this downstream position, explaining why the effect on the leakage velocity is less important.

The leakage velocity drop is not observed for case C, which coincides with no visible TLV/blade interaction.

In summary, the extraction of the leakage velocity brings two interesting results:

1. The TLV/blade interaction is detectable through a sudden drop of the leakage velocity along the chordwise direction.

2. A correlation may be sought between the position and magnitude of the leakage velocity drop and the occurrence of vortex breakdown. In our case, the intensity of the TLV and its interaction with the blade close to the leading edge for case A seem to promote the phenomenon. Case B is really interesting since it constitutes an intermediate case between cases A and C: the TLV/blade interaction occurs and leads to the same sudden leakage velocity drop but no vortex breakdown is observed. More configurations should be investigated to assess this correlation. RANS approaches are probably poorly adapted to investigate this phenomenon, which involves complex turbulent / vortex interactions.

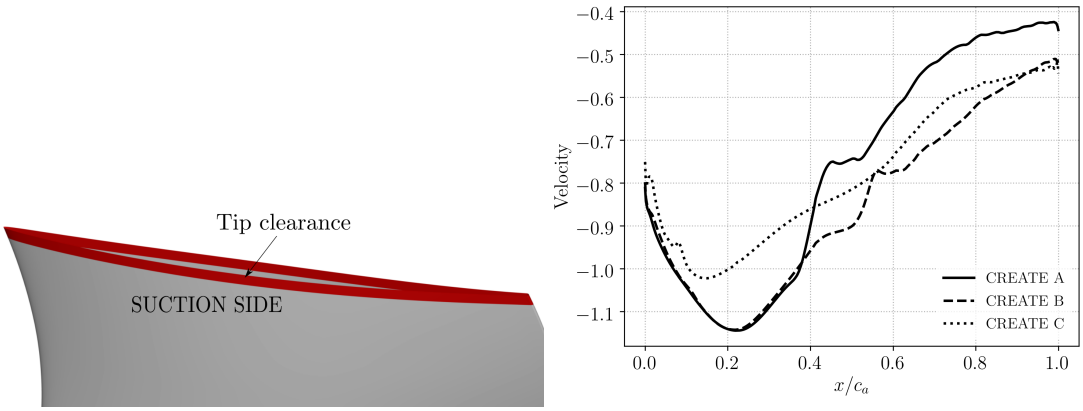

(a) Clearance zone

(b) Leakage velocity

Figure 7: **(a) Clearance zone (in red): the leakage velocity is extracted on the corresponding suction side of this zone. (b) Normalized averaged pitchwise component of the relative velocity (leakage velocity) within the clearance, with the rotor tip speed.**

3.2.3 Spectrum

The power spectral density (PSD) of the static pressure is compared between the three tip gap sizes in order to compare the distribution of energy in the spectra. Figure 8 shows the power spectral density (PSD) as a function of the frequency and the Strouhal number St_τ, calculated with the respective blade tip gap size of each case. The PSD is expressed as a gain:

$$G_{dB} = 10 \log_{10} \left(\frac{PSD(p_s)}{p_{ref}^2} \right) \quad \text{with: } p_{ref} = 2 \cdot 10^{-5} \,\text{Pa} \tag{2}$$

The three distributions follow the $-7/3$ slope on the spectrum decrease, also indicated (in green) in the figure. Indeed, in the inertial subrange, George *et al.* [9] analytically showed that the turbulent pressure fluctuations decrease with such a slope. First, and coherently with all the observations made before, the energy levels are higher for the two largest tip gaps (A and B). Moreover, the distributions are very similar for those two cases, while the levels for case C are much lower. Also, when normalizing by the tip gap size τ, the spectra for the two larger gaps coincide well, while the spectrum for case C is shifted to the left. A slight bump can be

observed around $St_\tau = 0.1$ for cases A and B, suggesting an unsteadiness driven by the tip gap length scale. It is worth reminding that a TLV/blade interaction has been observed for cases A and B, which could explain the higher levels of fluctuations and the spectrum hump around $St_\tau = 0.1$, as can be seen in Figure 6 in the 95% c_a plane cut at the tip.

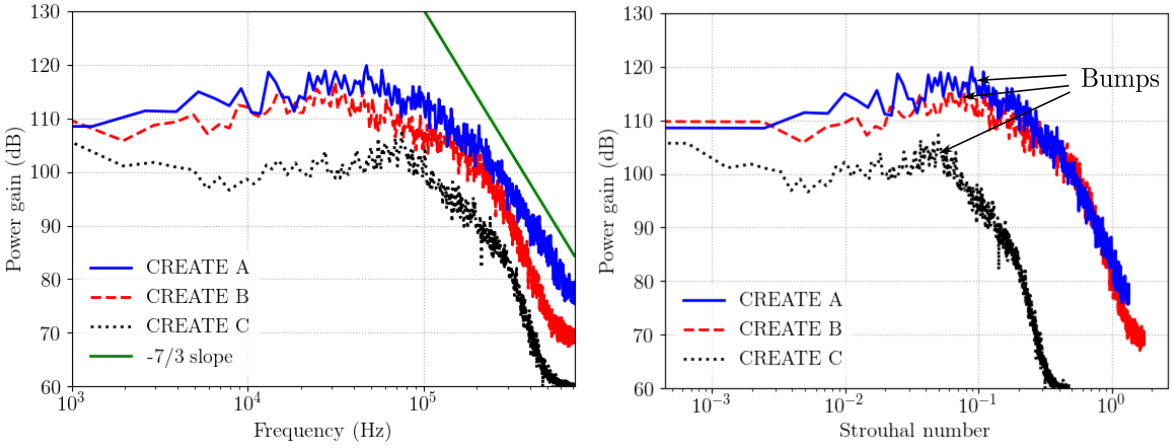

(a) (b)

Figure 8: **Power spectral density of the static pressure expressed in dB as a function of the frequency and the Strouhal number $St_\tau = \frac{f\tau}{U_{tip}}$ based on the respective tip gap size of each case.**

4 CONCLUSIONS

The third rotor of a high-pressure compressor has been simulated using a ZDES approach with the aim of investigating the effect of the tip gap size on the tip-leakage flow (TLF), in nominal operating conditions. Despite the differences in the first 70% height between the experiment and the numerical simulation on the larger tip gap, the results in the region of interest (the tip) are in fair agreement.

This allows a tip gap size sensitivity study to be carried out with the same inlet and outlet boundary conditions. The radial profiles indicate a more intense blockage for increasing gaps. The tip flow analysis has shown the classical structures of the TLF, from the detachment of the TLV on the suction side to the formation of the induced vortex and the tip-separation vortices downstream. The ZDES approach is interesting since it completely resolves the TLV with LES from where it detaches, showing a larger vortex with a larger gap. The flow topology also suggests a vortex breakdown for the largest gap, with the most energetic turbulent structures dividing into smaller structures in that case. The observation is confirmed by the vorticity magnitude evolution along the rotor passage.

The visualizations of the turbulent levels along the chord put in evidence a TLV/blade interaction in the clearance for the two larger gaps, very similar to the double-leakage tip clearance flow observed on another compressor in nominal operating conditions. The evolution of the leakage velocity in the clearance showed a clear link between the impact and a sudden drop of the leakage velocity from there. This drop is observed in cases A and B but the drop occurs closer to the leading edge and with a greater intensity for the larger gap. This may constitute a criterion on the occurrence of the vortex breakdown, being revealed by the Q-criterion views

in case A, but not in case B. Finally, concerning the wall pressure spectrum at tip, similar distributions and higher levels have been observed in the large gap cases where the TLV/blade interaction occurs.

ACKNOWLEDGEMENTS

This work was granted access to the HPC resources of CCRT from CEA, and to the HPC resources of CINES through the allocation 2018-A0052A10277 attributed by GENCI (Grand Equipement National de Calcul Intensif). The simulations have been carried out in the framework of the *elsA* three-party agreement between Airbus, Safran and ONERA, co-owners of the software.

References

[1] H. Brandt, L. Fottner, H. Saathoff, and U. Stark. Effects of the Inlet Flow Conditions on the Tip Clearance Flow of an Isolated Compressor Rotor. In *Volume 5: Turbo Expo 2002, Parts A and B*, pages 1123–1132, Amsterdam, The Netherlands, Jan. 2002. ASMEDC.

[2] N. Courtiade. *Experimental analysis of the unsteady flow and instabilities in a high-speed multistage compressor*. PhD, Ecole Centrale de Lyon, Nov. 2012.

[3] N. Courtiade and X. Ottavy. Experimental Study of Surge Precursors in a High-Speed Multistage Compressor. *Journal of Turbomachinery*, 135(6):061018 (9 pp.), Sept. 2013.

[4] I. J. Day. Fundamentals of Stall and Surge. pages 1–55, Von Karman Institute, 1992.

[5] S. Deck. Recent improvements in the zonal detached eddy simulation (ZDES) formulation. *Theoretical and Computational Fluid Dynamics*, 26(6):523–550, 2012.

[6] J. Denton. Loss Mechanisms in Turbomachines. Technical report, The American Society of Mechanical Engineers, New York, 1993.

[7] B. Deveaux, C. Fournis, V. Brion, J. Marty, and A. Dazin. Experimental analysis and modeling of the losses in the tip leakage flow of an isolated, non-rotating blade setup. *Experiments in Fluids*, 61(5):1–23, 2020. Publisher: Springer.

[8] A. Doukelis, K. Mathioudakis, and K. Papailiou. The effect of tip clearance gap size and wall rotation on the performance of a high-speed annular compressors cascade. *The American Society of Mechanical Engineers*, (98-GT-98):1–8, 1998.

[9] W. K. George, P. D. Beuther, and R. E. Arndt. Pressure spectra in turbulent free shear flows. *J. Fluid Mech*, 148:155–191, 1984.

[10] C. Hah. Effects of double-leakage tip clearance flow on the performance of a compressor stage with a large rotor tip gap. *Journal of Turbomachinery*, 139(6), 2017. Publisher: American Society of Mechanical Engineers Digital Collection.

[11] M. Hewkin-Smith, G. Pullan, S. D. Grimshaw, E. M. Greitzer, and Z. S. Spakovszky. The Role of Tip Leakage Flow in Spike-Type Rotating Stall Inception. In *Volume 2D: Turbomachinery*, page V02DT46A009, Charlotte, North Carolina, USA, June 2017. American Society of Mechanical Engineers.

[12] M. Inoue, M. Kuroumaru, and M. Fukuhara. Behavior of Tip Leakage Flow Behind an Axial Compressor Rotor. *Journal of Engineering for Gas Turbines and Power*, 108(1):7–14, Jan. 1986.

[13] S. Kang and C. Hirsch. Tip leakage flow in linear compressor cascade. *Journal of Turbomachinery*, 116:657–664, 1994.

[14] S. A. Khalid, A. S. Khalsa, I. A. Waitz, C. S. Tan, E. M. Greitzer, N. A. Cumpsty, J. J. Adamczyk, and F. E. Marble. Endwall Blockage in Axial Compressors. *Journal of Turbomachinery*, 121:499–509, 1999.

[15] J. Marty and C. Uribe. Impact of Underlying RANS Turbulence Models in Zonal Detached Eddy Simulation: Application to a Compressor Rotor. *International Journal of Turbomachinery, Propulsion and Power*, 5(3):22, Aug. 2020.

[16] C. Montsarrat, J. Marty, J. Boudet, E. Lippinois, and X. Ottavy. Hybrid (ZDES) simulation of tip-leakage flow in an axial compressor. Gdansk, July 2019.

[17] D. A. Rains. *Tip clearance Flows in Axial Compressors and Pumps*. PhD Thesis, California Institute of Technology, Pasadena, California, 1954.

[18] W. Riéra, J. Marty, L. Castillon, and S. Deck. Zonal detached-eddy simulation applied to the tip-clearance flow in an axial compressor. *AIAA Journal*, pages 2377–2391, 2016.

[19] P. Sagaut, S. Deck, and M. Terracol. *Multiscale and Multiresolution Approaches in Turbulence*. Imperial College Press, 2006.

[20] P. Spalart. Strategies for turbulence modelling and simulations. *International Journal of Heat and Fluid Flow*, 2000.

[21] P. Spalart and S. Allmaras. A one-equation turbulence model for aerodynamic flows. In *30th Aerospace Sciences Meeting and Exhibit*, Reno,NV,U.S.A., Jan. 1992. American Institute of Aeronautics and Astronautics.

[22] H. D. Vo, C. S. Tan, and E. M. Greitzer. Criteria for spike initiated rotating stall. *Journal of turbomachinery*, 130(1):011023, 2008.

[23] Y. Wu and W. Chu. Behaviour of tip-leakage flow in an axial flow compressor rotor. *Proceedings of the Institution of Mechanical Engineers, Part A: Journal of Power and Energy*, 221(1):99–110, Feb. 2007.

[24] D. You, M. Wang, P. Moin, and R. Mittal. Large-eddy simulation analysis of mechanisms for viscous losses in a turbomachinery tip-clearance flow. *Journal of Fluid Mechanics*, 586:177–204, Apr. 2007.

[25] H. Zhang, X. Deng, F. Lin, J. Chen, and W. Huang. A study on the mechanism of tip leakage flow unsteadiness in an isolated compressor rotor. In *Turbo Expo: Power for Land, Sea, and Air*, volume 4241, pages 435–445, 2006.